Infrared Spectra, Integrated Band Intensities, and Anharmonic Force Field of $H_2C{=}CHF$

Paolo Stoppa,* Andrea Pietropolli Charmet, Nicola Tasinato, and Santi Giorgianni

Dipartimento di Chimica Fisica, Università Ca' Foscari di Venezia, Calle Larga S. Marta 2137, I -30123 Venezia, Italy

Alberto Gambi

Dipartimento di Scienze e Tecnologie Chimiche, Università degli Studi di Udine, Via Cotonificio 108, I-33100 Udine, Italy

Received: September 26, 2008

The gas-phase infrared spectra of vinyl fluoride, $H_2C{=}CHF$, have been examined at medium resolution in the range 400−8000 cm^{-1}. The assignment of the absorptions in terms of fundamental, overtone, and combination bands, assisted by quantum chemical calculations, is consistent all over the region investigated. Spectroscopic parameters, obtained from the analysis of partially resolved rotational structure of some bands, have been derived and compared with the corresponding calculated values. Accurate values of integrated band intensities have also been determined for the first time. High-level *ab initio* calculations with large basis sets have been performed. Correlated harmonic force fields have been obtained from coupled cluster CCSD(T) calculations with the cc-pVQZ basis set, while anharmonic force constants have been computed employing the less resource demanding cc-pVTZ basis set. A good agreement between the computed and the experimental data has been obtained including those for the integrated infrared band intensities.

1. Introduction

Vinyl fluoride, mainly employed as a monomer for the production of synthetic resins such as poly(vinyl fluoride), has been studied extensively by spectroscopic methods. Low resolution infrared investigations, mainly limited to the identification of the fundamental modes, have been carried out a long time ago,[1−3] and a detailed analysis of the partially resolved structure has been only performed around 900 cm^{-1} for the ν_8, ν_{10}, and ν_{11} modes perturbed by Coriolis resonance.[4] Ground-state parameters, obtained from the analysis of microwave spectra,[5−7] have been more extensively determined combining the microwave data available in the literature together with infrared combination differences.[8] Many investigations have been also devoted to the determination of its structure (see, for example, ref 9 and references therein), and a semiexperimental equilibrium structure has been derived[10] from experimental ground-state rotational constants and rovibrational interaction parameters calculated from an *ab initio* anharmonic force field.

In the last years there has been an increased interest in spectroscopic studies of haloalkenes owing to their potential role as air pollutants and also to improve the theoretical studies of their reactivity toward hydroxyl radical and ozone (see, for example, refs 11 and 12 and references therein). The high resolution infrared spectra of vinyl fluoride have been investigated by this research group in many spectral regions,[13−17] and the achieved results have led to the determination of accurate molecular parameters for several fundamentals and overtone vibrations, and to a better understanding of the interaction mechanism for the observed perturbations.

The present work deals with a more complete vibrational study of vinyl fluoride at medium resolution in the 400−8000 cm^{-1} spectral region. The absorption features have been interpreted in terms of fundamental, overtone, and up to three-quanta combination bands, and the absolute infrared photoabsorption cross sections have been measured for the first time.

Accurate *ab initio* calculations of the harmonic and anharmonic force fields have been also performed. The present work improves previous theoretical studies by using the coupled cluster CCSD(T) approach in combination with large basis sets.

2. Experimental Details

The sample of $H_2C{=}CHF$ (purity ≈ 99%), obtained commercially from Peninsular Chemical Research, Inc., has been used without further purification.

The spectra have been recorded on the Bruker Vertex 70 FTIR spectrometer at a resolution between 0.2 and 1.0 cm^{-1} in the 400−5000 cm^{-1} range and at 1.0 cm^{-1} in the 5000−8000 cm^{-1} range. The wavenumber accuracy in the range investigated (400−8000 cm^{-1}) has been estimated to be around 0.2 cm^{-1}. A 134.0 (±0.5) mm path length, double walled, stainless steel gas cell equipped with KBr windows has been employed in the range 400−5000 cm^{-1}, while a multipass cell (150−3750 cm, CaF_2 windows) has been used in the NIR region. A total of 128 scans for both the sample and the background spectra have been coadded and transformed into the corresponding absorbance or transmittance spectrum using boxcar apodization function and Mertz phase correction.

For the vibrational analysis, the sample pressures have been varied in the range 0.37−40 kPa, and the spectra have been recorded at room temperature. For the absorption cross section measurements (400−3500 cm^{-1}), the temperature in the cell, continuously monitored by thermocouples, has been kept constant at 298.0 K (±0.5 K). Different pressures of vinyl fluoride have been used, for both the pure compound and its mixture with N_2 (SIAD, purity >99%) to a total pressure of 101 kPa. Pressure measurements have been performed employ-

* To whom correspondence should be addressed. E-mail: stoppa@unive.it.

10.1021/jp808556e CCC: $40.75
Published on Web 02/02/2009

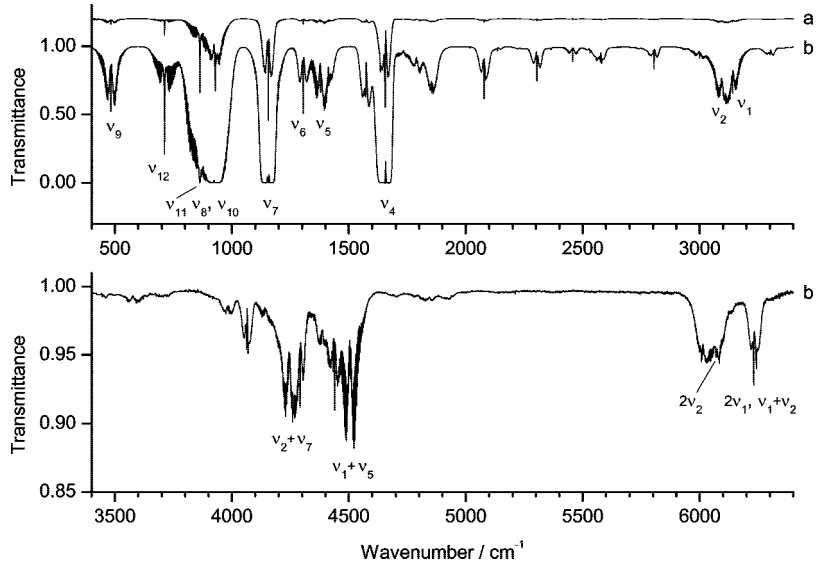

Figure 1. Gas-phase IR spectra of $H_2C{=}CHF$ at 1.0 cm^{-1} resolution: (a) path length 13.4 cm, pressure = 613 Pa and (b) path length 13.4 cm, pressure = 11.4 kPa. Only some representative bands are labeled. For a better reading, the a trace has been shifted upward.

ing capacitance vacuum gauges (Alcatel model ARD 1001, 1002, and 1003 with a full scale range of 1013, 101, and 10 mbar, respectively), each with a quoted manufacturer's full scale accuracy of 0.15%. A 15 min delay has been adopted between the filling of the cell and the recording of the corresponding spectrum. The gas cell has been evacuated to about 10^{-4} Pa before and after each sample measurement by means of a diffusion pump backed by a double stage rotary pump, and the corresponding background spectra have been acquired. Adsorption of the gas sample on the cell walls has been checked both by directly measuring the pressure and by monitoring the absorption spectrum; it has been found negligible over a period of 2 h, which is far longer than the typical time required to obtain a spectrum.

3. Computational Details

Quantum-chemical calculations have been carried out at the correlated levels of coupled cluster theory with single and double excitations[18] augmented by a perturbational estimate of the effects of connected triple excitations, CCSD(T).[19] The Dunning's correlation consistent polarized valence basis sets, cc-pVTZ and cc-pVQZ,[20,21] have been employed.

The cc-pVTZ basis set is described by a [4s3p2d1f/3s2p1d] contraction of a (10s5p2d1f/5s2p1d) primitive set for C, F/H atoms, whereas the cc-pVQZ basis set corresponds to a [5s4p3d2f1g/4s3p2d1f] contraction of a (12s6p3d2f1g/6s3p2d1f) primitive set. The frozen core approximation, where the carbon and fluorine 1s-like molecular orbitals have been constrained to remain doubly occupied in the CCSD(T) calculations, has been applied. Spherical harmonic angular functions have been used throughout.

At first the molecular geometry of vinyl fluoride has been optimized within the constraint of C_s point group symmetry at the CCSD(T)/cc-pVTZ level of theory. At the computed equilibrium geometry, harmonic force field has been evaluated analytically employing the same level of theory. The CCSD(T)/cc-pVTZ cubic and quartic normal coordinates force constants (φ_{ijk}, φ_{ijkk}) have been determined with the use of a finite difference procedure[22] involving displacements along the normal coordinates (step size 0.05 $amu^{1/2}$ bohr). All these calculations have been performed with a local version of the Mainz−Austin−Budapest version of the ACES II program package.[23]

Since the semiexperimental structure of vinyl fluoride is in good agreement with the structure calculated at the CCSD(T)/cc-pVQZ level of theory,[10] an additional geometry optimization followed by the harmonic force field evaluation has been performed at this level of theory. These calculations have been carried out with the MOLPRO system of programs,[24] where the Hessian matrix is calculated numerically by finite differences.[25]

4. Results and Discussion

4.1. Spectral Data and Assignment. Survey spectra of vinyl fluoride in the regions investigated, recorded at 1.0 cm^{-1} resolution, are shown in Figure 1. Few assignments are given below selected bands in order to facilitate the reading of the spectra, which provide a rich source of information on overtone and combination levels. The frequencies and the assignments for the observed bands are given in Table 1. Because of its C_s symmetry, the $H_2C{=}CHF$ molecule originates two kinds of absorption. The vibrations with A' symmetry species give rise to A-/B-hybrid bands with different contributions of the components. The A'' vibrations produce C-type band envelopes having well defined central Q branch.

All the fundamentals, except the CH stretchings (ν_1, ν_2, and ν_3 modes), have been extensively analyzed at high resolution (13−17). The ν_1 and ν_2 fundamentals, although partially overlapped, show a predominant B-type structure. The ν_3 is very weak and overlapped by the stronger ν_2. Table 2 reports for all the fundamentals the experimental frequencies together with their calculated values. The wavenumbers of the ν_3, ν_4, and ν_5 fundamentals have been computed after diagonalization of the matrices in which Fermi resonances have been taken into account. There is an overall good agreement between the calculated and observed frequencies. In addition, the same table reports the approximate description of the normal modes based on the total energy distribution (see later).

In the most favorable experimental conditions, a lot of overtones and combination bands could be observed and positively identified. The proposed assignments (Table 1) have been made considering the calculated anharmonicity constants, the relative intensity, and the expected band contour of the combined normal vibrations. The assignment appears to be consistent throughout the entire spectral region investigated.

TABLE 1: Observed Band Centers (cm^{-1}) of the Gas-Phase IR Spectra of $H_2C{=}CHF$

band	observed envelope	relative intensity [a]	wavenumber [b]
ν_9	A/B	m	482.9
$2\nu_9 - \nu_9$			485.5
ν_{12}	C	m	712.4 ± 0.2
$\nu_9 + \nu_{12} - \nu_9$			713.5
ν_{11}	C	s	863.1 ± 0.2
$\nu_9 + \nu_{11} - \nu_9$			864.3 ± 0.2
ν_8	A/B	s	927.8 ± 0.2
ν_{10}	C	s	929.1 ± 0.2
$\nu_7 + \nu_9 - \nu_9$			1152.7
ν_7	A	vs	1155.4
ν_6	A	w	1305.2
ν_5	A/B	m	1379.5
$2\nu_{12}$		vw	1424.4
$\nu_{11} + \nu_{12}$	A/B	w	1574.3 ± 0.5
$\nu_7 + \nu_9$		vw	1635.7
$\nu_4 + \nu_9 - \nu_9$			1652.8
ν_4	A	vs	1655.6
$\nu_{10} + \nu_{11}$	B/A	w	1790.3
$2\nu_8$	A/B	w	1854.6
$\nu_7 + \nu_9 + \nu_{11} - \nu_9$			2017.7
$\nu_7 + \nu_{11}$	C	vw	2018.6
$\nu_7 + \nu_8 + \nu_9 - \nu_9$			2075.6
$\nu_7 + \nu_8$	A	w	2077.7
$\nu_4 + \nu_9$	A	vw	2136.2
$2\nu_7$	A	vw	2304.1
$\nu_6 + \nu_7$	A	vw	2457.5
$\nu_5 + \nu_7$	A	vw	2530.7
$2\nu_6$		vw	2608.3
$2\nu_5$	A/B	vw	2751.8
$\nu_4 + \nu_7$	A	vw	2805.1
$\nu_4 + \nu_6$		vw	2949.6 ± 0.5
$\nu_4 + \nu_5$	A	w	3000.3
ν_2	B/A	w	3094.5
ν_1	A/B	w	3140.7
$2\nu_4$	A	vw	3301.6 ± 0.5
$\nu_1 + \nu_8$	A/B	vw	4063.9
$\nu_2 + \nu_7$	B/A	vw	4246.0
$\nu_1 + \nu_7$	A/B	vw	4292.9
$\nu_1 + \nu_6$	A/B	vw	4439.7
$\nu_1 + \nu_5$	B/A	w	4505.6
$\nu_1 + 2\nu_5$	A/B	vw	5863.8 ± 0.5
$2\nu_2$	A/B	vw	6070.1 ± 0.5
$\nu_2 + \nu_3$	A/B	vw	6120.3 ± 0.5
$\nu_1 + \nu_2$	A/B	vw	6230.7 ± 0.5
$2\nu_1$	A/B	vw	6243.2 ± 0.5
$\nu_1 + \nu_2 + \nu_6$	A/B	vw	7531.1 ± 0.5
$2\nu_1 + \nu_5$	A/B	vw	7589.0 ± 0.5
$\nu_1 + \nu_2 + \nu_5$		vw	7603.0 ± 0.5

[a] Abbreviations used are as follows: vs = very strong, s = strong, m = medium, w = weak, vw = very weak. [b] The experimental error is ±0.1 cm^{-1} unless otherwise quoted.

The presence of satellite peaks near the band origin of some fundamentals and combination bands provide further information on the vibrational energy levels of the hot bands $\nu_i + \nu_j - \nu_j$ and $\nu_i + \nu_j + \nu_k - \nu_j$, where the ν_j is the vibrational level with $v_9 = 1$ at about 483 cm^{-1}.

4.2. Rotational Analysis. In the spectra recorded at the highest resolution (0.2 cm^{-1}), a number of bands exhibit resolved rotational structure which could be assigned and analyzed. From the rotational constants,[8] the parameter $2(A - \bar{B}) = 3.65$ cm^{-1}, where $\bar{B} = (B + C)/2$, is obtained, and this value is so large that the B- and C-type bands can exhibit resolved rotational structure similar to that present in the perpendicular bands of symmetric tops. Indeed, since the separation between consecutive peaks is around 3.6 ± 0.1 cm^{-1}, the observed structure has to be attributed to the ${}^{p,r}Q_K$ clusters of B- or C-type bands.

The analysis has been carried out by the usual least-squares fitting procedure using, in the approximation for symmetric tops, the following reduced equation

$$\tilde{\nu}^{P,R} = \tilde{\nu}_0 + (A' - \bar{B}') \mp 2(A' - \bar{B}')K + [(A' - \bar{B}') - (A'' - \bar{B}'')]K^2 \quad (1)$$

where the upper and lower signs refer to the P- and R-branch clusters, respectively.

The rotational analysis has been performed only for the bands not yet investigated under high resolution. Then, the study has been carried out on the B-type component of the ν_1 and ν_2 fundamentals and $\nu_1 + \nu_5$, $\nu_4 + \nu_5$, and $\nu_6 + \nu_7$ combination bands. The band origins ($\tilde{\nu}_0$), the rotational parameters, the number of data used in the least-squares fit, and the obtained standard deviations for all the five bands considered are summarized in Table 3. Figure 2 shows the rotational details of the ν_1 and ν_2 bands in the region around 3000 cm^{-1}. Some assignments of the ${}^{p}Q_K$ and ${}^{r}Q_K$ features of the ν_1 fundamental are also indicated. The observed lines undergoing asymmetry splitting have not been used in the fitting procedure. Frequencies have been usually taken at the top of the sharp lines. The ${}^{r}Q_K$ heads of ν_2 are severely mingled with the ${}^{p}Q_K$ series of the ν_1 band. In order to verify the consistency of the assigned rotational structure, checks have been performed by using the ground-state combination difference method in the symmetric top limit.

4.3. Integrated Band Intensities. According to the Beer−Lambert law, the absorbance cross section per molecule (cm^2 $molecule^{-1}$) of the sample, $\sigma(\tilde{\nu})$, has been calculated from the measured infrared absorbance

$$\sigma(\tilde{\nu}) = \frac{A(\tilde{\nu}) \ln 10}{Nl} \quad (2)$$

where $A(\tilde{\nu})$ is the absorbance (at wavenumber $\tilde{\nu}$) of an optical path length l (cm) and N is the number density (molecule cm^{-3}). Assuming the validity of the ideal gas law, in the range of the pressures used in the present work N is related to the pressure and the temperature by

$$N = \frac{10^{-6} P N_A}{RT} \quad (3)$$

where R is the molar gas constant (J K^{-1} mol^{-1}), P is the pressure (Pa), N_A is Avogadro's constant, and T is the temperature (K). The integrated cross section G_{int} (cm^2 $molecule^{-1}$ cm^{-1}) is then derived from the absorbance cross section by the following equation

$$G_{int} = \int_{\tilde{\nu}_1}^{\tilde{\nu}_2} \sigma(\tilde{\nu})\, d\tilde{\nu} = \frac{10^6 RT \ln 10}{N_A l P} \int_{\tilde{\nu}_1}^{\tilde{\nu}_2} A(\tilde{\nu})\, d\tilde{\nu} \quad (4)$$

where $\tilde{\nu}_1$ and $\tilde{\nu}_2$ are the integration limits corresponding to the wavenumbers where the absorption is negligible. If two or more strongly overlapped bands without a clear separation were present in the spectral interval, a single integration has been performed. As suggested by Nemtchinov and Varanasi,[26] the experimental uncertainty in the cross-section measurements has been estimated by taking into account the uncertainties of the pressure and temperature of the sample, of the optical path length, of the photometric accuracy of the FTIR spectrometer, and of the evaluation of the absorbance.

At the beginning of the experiments, some spectra have been recorded at two different resolutions (0.2 and 0.5 cm^{-1}) for

TABLE 2: Gas-Phase Fundamentals of H_2C=CHF

symmetry species	mode	approximate description	observed band center (cm^{-1})	calculated[a] band center (cm^{-1})
A′	ν_1	CH_2 antisym. stretch	3140.7	3136.7
	ν_2	CH stretch	3094.5	3084.9
	ν_3	CH_2 sym. stretch	3062.1[b]	3073.1/3040.8[c]
	ν_4	C=C stretch	1655.6	1653.9/1657.1[c]
	ν_5	CH_2 bend	1379.5	1375.5/1378.7[c]
	ν_6	CH bend	1305.2	1304.0
	ν_7	CF stretch	1155.4	1155.7
	ν_8	CH_2 rock	927.8	927.5
	ν_9	C=CF bend	482.9	480.4
A″	ν_{10}	torsion	929.1	930.2
	ν_{11}	CH_2 wag	863.1	854.6
	ν_{12}	CH out of plane bend	712.4	712.9

[a] From the hybrid anharmonic force field (see text). [b] From Raman spectrum of the gas.[3] [c] Fermi perturbed/unperturbed values.

TABLE 3: Molecular Parameters (cm^{-1}) of H_2C=CHF Bands[a]

band	$\tilde{\nu}_0$	$(A' - \bar{B}')$	$(A'' - \bar{B}')$	no. of data	σ^b
ν_1	3140.99(6)	1.8145(18) 1.8202[c]	1.8235(19)	20	0.14
ν_2	3096.46(3)	1.7958(16) 1.8198[c]	1.8200(17)	18	0.07
$\nu_1 + \nu_5$	4505.45(3)	1.8164(11) 1.8285[c]	1.8145(11)	27	0.10
$\nu_4 + \nu_5$	2999.68(6)	1.824(3) 1.826[c]	1.819(3)	14	0.12
$\nu_6 + \nu_7$	2457.57(3)	1.8119(10) 1.8270 [c]	1.8128(10)	24	0.09
		average:	1.8180(17) 1.8261[c]		

[a] The uncertainties given in parentheses are one standard deviation of the last significant digit. [b] Standard deviation (cm^{-1}). [c] Calculated values from the quadratic CCSD(T)/cc-pVQZ and cubic CCSD(T)/cc-pVTZ force constants.

different pressures of both the pure vinyl fluoride and its mixture with N_2. A linear dependence of the absorbance with the pressure of the sample has been observed over all the concentration range used. The calculated band intensities corresponding to the same concentration of the sample at different spectral resolutions have been found to be equal within the error of the measurements; therefore, we have chosen to determine the integrated cross sections from the spectra of the pure gas (pressures in the range 4−33 hPa) measured at the resolution of 0.5 cm^{-1} because they generally have a better signal-to-noise ratio, especially for the weaker absorption features.

Taking into account the different intensities of the absorption bands in the range 400−3500 cm^{-1}, the infrared spectra of vinyl fluoride have been divided into three main regions. The first, located between 400 and 780 cm^{-1}, is characterized by the weak absorptions originating from the ν_9 (at 483 cm^{-1}) and the ν_{12} (at 712 cm^{-1}). The second range, located between 780 and 1700 cm^{-1}, shows several strong bands (ν_8, ν_{10}, ν_{11}, ν_7, and ν_4) and two weaker absorptions (ν_5 and ν_6). Finally, the spectrum between 1700 and 3500 cm^{-1} contains many very weak features, corresponding to the CH stretching fundamentals (ν_1, ν_2, and ν_3) and various combination and overtone bands.

By using eqs 2−4, the integrated absorption cross sections have been determined, and the resulting averaged values, together with their statistical errors, are reported in Table 4; the estimated experimental uncertainty in the integrated cross sections is better than 6.0%. For completeness, the same table also includes the calculated intensity values. As it can be seen, the overall agreement is rather good being the greatest difference about 22%. Figure 3 shows the resulting averaged spectrum for the region investigated in the present analysis.

4.4. Equilibrium Geometry and Harmonic Force Constants. A detailed analysis of the equilibrium structure of vinyl fluoride with the determination of its semiexperimental structure has been reported recently by Demaison.[10] In general, CCSD(T) calculations give very reliable results in the determination of the equilibrium geometry. The systematic errors, on the basis of several structure optimizations, give an accuracy of 0.005 Å for bond lengths and 0.2° for bond angles.[27] From these considerations a geometry optimization has been carried out at the CCSD(T)/cc-pVTZ level of theory using the analytical gradients and the analytical derivatives of the dipole moment to compute the integrated infrared band intensities.

The harmonic force field has also been evaluated at the same level of theory from analytical second derivatives. On the basis of the structure calculations of ref 10, we have also performed the CCSD(T)/cc-pVQZ geometry optimization. Assuming the CCSD(T)/cc-pVQZ optimized equilibrium structure as the nearest to the true molecular geometry, the harmonic force field has been evaluated at the same level of theory in a Cartesian coordinates representation.

For the sake of completeness, Table 5 collects the set of 12 chemically intuitive internal coordinates R. Of them, the planar (R_1−R_9) coordinates correspond to the nine determinable structural parameters which define the geometry of H_2C=CHF. Table 6 summarizes the fundamental frequencies computed with the harmonic force fields determined at the two levels of theory taken into account. The total energy distribution (TED %) values[28] in terms of the internal coordinates of Table 5 are also reported.

The integrated infrared band intensities, in units of km/mol, have been computed employing the formula

$$A_i = 42.254\ 72\left|\frac{\partial \mu}{\partial Q_i}\right|^2 \qquad (5)$$

where $\partial\mu/\partial Q_i$ are the dipole moment derivatives in D/(Å amu$^{1/2}$) evaluated via analytical derivatives computed at the CCSD(T)/cc-pVTZ level of theory. These data are also included in Table 6.

4.5. Ab Initio Anharmonic Force Field. The theoretical anharmonic force field has been calculated at the CCSD(T) level of theory using the ACES II program.[23] The cc-pVTZ basis set has been used in the frozen core approximation. Equilibrium molecular geometry has been calculated at first; then, the associate quadratic force constants have been evaluated analytically in the Cartesian coordinates. The cubic and quartic semidiagonal force constants have been calculated in the reduced

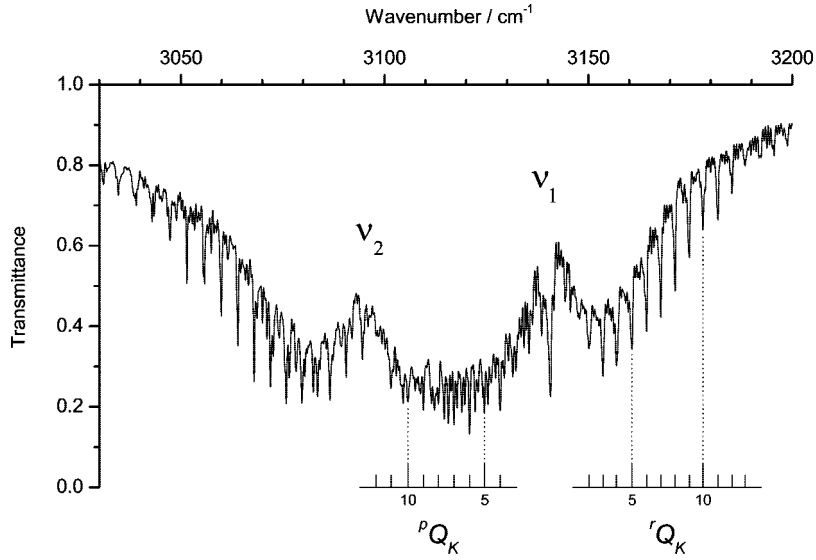

Figure 2. Gas-phase IR spectrum of the CH stretching region of $H_2C{=}CHF$ at 0.2 cm^{-1} resolution (path length 13.4 cm, pressure = 3213 Pa, room temperature). The B-type rotational structure of the ν_1 band is labeled.

TABLE 4: Integrated Cross Sections of $H_2C{=}CHF$ in the Range 400 − 3500 cm^{-1}

	integrated absorption cross sections		
integration limits (cm^{-1})	experimental[a] ($\times 10^{18}$ cm^2 $molecule^{-1}$ cm^{-1})	experimental[a] (km/mol)	theoretical[b] (km/mol)
420−580	0.714(12)	4.30(7)	4.24
610−1050	18.33(11)	110.4(7)	111.51
1050−1250	12.93(12)	77.9(7)	87.07
1250−1480	1.242(18)	7.48(11)	9.06
1520−1720	13.9(2)	83.7(12)	101.71
2000−2200	0.356(6)	2.14(4)	1.68
2900−3420	1.59(3)	9.57(18)	11.68

[a] Standard deviations in units of the last significant digit are given in parentheses. The estimated experimental uncertainties are better than 6.0% of the reported value. [b] Sum of the computed intensities of the fundamentals comprised in the integration limits (see Table 6).

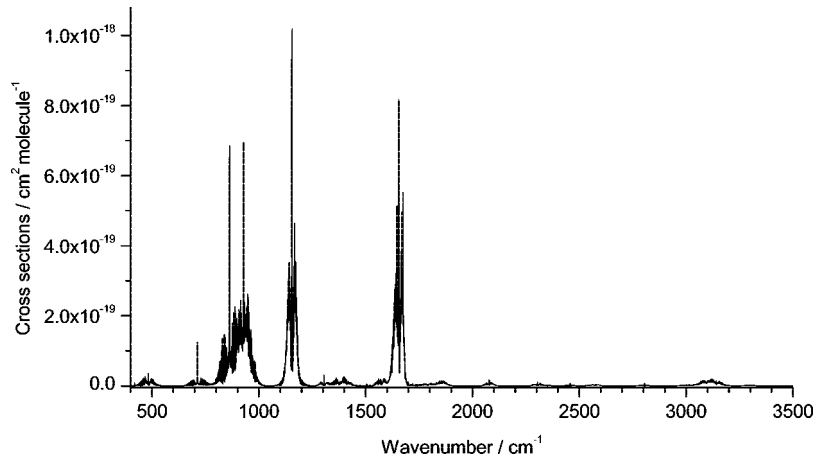

Figure 3. Averaged absorption cross-section spectrum of $H_2C{=}CHF$ in the region 400−3500 cm^{-1} (0.5 cm^{-1} resolution, T = 298 K).

normal coordinates space with the use of a finite differences procedure, involving displacements along normal coordinates, through the calculation of analytic second derivatives at these displaced geometries.

As previously reported, the CCSD(T)/cc-pVQZ calculations of geometry and harmonic force field are assumed to better the approach to the experimental values. However, in order to reduce the considerable amount of computer time required to obtain cubic and quartic force constants at this level of theory, a hybrid force field having the geometry and second-order force constants at the CCSD(T)/cc-pVQZ level of theory and the cubic and semidiagonal quartic force constants determined at CCSD(T)/cc-pVTZ has been employed. Therefore, the anharmonic spectroscopic constants have been derived from this hybrid theoretical normal coordinates force field applying standard formulas based on second-order rovibrational perturbation theory.[29,30]

4.6. Anharmonicity Constants and Vibrational Resonances. The anharmonicity constants x_{ij} of vinyl fluoride, calculated with the force field previously described, are reported in Table 7; these constants depend on the quadratic, cubic, and quartic force constants. Strong anharmonic interactions between fundamentals and overtones or combination bands may lead to a breakdown of the corresponding perturbational formulas. In these cases it is necessary to consider the x_{ij} effective constants

TABLE 5: Definition of the Internal Coordinates of $H_2C{=}CHF$ in the C_s Symmetry Point Group and Theoretical Equilibrium Geometries Compared to the Semiexperimental Molecular Structure (Bond Lengths in Å, Bond Angles in deg)

			cc-pVTZ	cc-pVQZ	semiexperimental [a]
A'	R_1	C−F	1.3430	1.3428	1.3428
	R_2	C=C	1.3285	1.3253	1.3210
	R_3	$C-H_c$ [b]	1.0808	1.0801	1.0789
	R_4	$C-H_g$ [b]	1.0818	1.0809	1.0789
	R_5	$C-H_t$ [b]	1.0797	1.0790	1.0774
	R_6	FCC	122.09	121.91	121.70
	R_7	CCH_c	121.34	121.39	121.34
	R_8	CCH_g	125.51	125.32	126.40
	R_9	CCH_t	119.05	118.93	118.97
A''	R_{10}	$C-H_g$ out-of-plane bending			
	R_{11}	$C-H_c$ out-of-plane bending			
	R_{12}	torsion			

[a] Reference 10. [b] c, *cis* to fluorine; g, geminal; t, *trans* to fluorine.

TABLE 6: Harmonic Wavenumbers ω_i, Total Energy Distribution (TED %), and Integrated Infrared Band Intensities Obtained for $H_2C{=}CHF$ at the CCSD(T) Level of Theory Used in the Calculations Employing the cc-pVTZ and cc-pVQZ Basis Sets

			cc-pVTZ		cc-pVQZ
	mode	TED %[a]	wavenumbers (cm^{-1})	intensities (km/mol)	wavenumbers (cm^{-1})
A'	ω_1	$R_5(55) + R_3(43)$	3280	1.96	3282
	ω_2	$R_4(92)$	3217	6.99	3221
	ω_3	$R_3(50) + R_5(44)$	3178	0.69	3178
	ω_4	$R_2(69)$	1703	93.08	1700
	ω_5	$R_9(48) + R_7(24) + R_8(23)$	1425	5.69	1418
	ω_6	$R_8(66) + R_7(20) + R_2(16)$	1335	2.50	1332
	ω_7	$R_1(51) + R_7(20) + R_6(20)$	1186	87.01	1179
	ω_8	$R_1(36) + R_9(32) + R_7(18)$	946	32.96	943
	ω_9	$R_6(78) + R_7(12)$	481	4.24	481
A''	ω_{10}	$R_{12}(100)$	956	35.58	954
	ω_{11}	$R_{11}(100)$	871	41.02	872
	ω_{12}	$R_{10}(96)$	725	1.95	725

[a] Terms ≥10%.

TABLE 7: Anharmonicity Constants x_{ij} (cm^{-1}) of $H_2C{=}CHF$[a]

$i \setminus j$	1	2	3	4	5	6	7	8	9	10	11	12
1	− 30.7	− 10.1	− 102.5	0.2	− 17.1	− 4.9	− 3.4	− 5.4	− 1.5	− 3.5	− 15.9	− 4.1
2		− 50.9	− 20.2	−3.5	1.5	− 13.1	− 3.6	0.4	− 0.3	− 12.8	−3.5	− 3.5
3			− 24.2	− 9.2* (16.1)	− 14.7* (10.6)	−4.9	− 3.6	− 4.5	− 1.1	− 4.6	− 8.8	− 4.2
4				− 3.5	− 9.2* (− 34.5)	− 12.5	− 7.3* (− 6.8)	−10.2	− 4.1* (− 3.5)	− 6.2* (− 5.6)	− 7.1* (− 20.5)	− 3.9* (− 3.3)
5					−3.8	− 5.9	− 3.4	− 4.6* (− 14.1)	− 0.6* (− 10.1)	−1.4	− 7.3	− 1.2* (− 6.1)
6						− 2.3	− 2.9	− 0.2	1.0	− 1.8	− 0.8	−1.4
7							− 3.2	− 5.3	− 2.1* (−2.7)	− 1.8	0.8	− 2.0
8								− 0.6	0.1* (9.6)	− 0.7	2.0	0.3
9									1.3	− 0.1	0.9	1.1
10										− 3.4	− 1.2	−0.7* (− 1.3)
11											2.0* (5.4)	− 1.2
12												− 0.6* (0.6)

[a] The constants which are affected by Fermi resonances are marked by an asterisk, and the corresponding unperturbed values are given in parentheses.

(values indicated by an asterisk in Table 7) excluding such contributions from the perturbational summations.[30] These effective anharmonicity constants have been here introduced to account for the following Fermi resonances: $2\nu_{11}/\nu_4$, $2\nu_{12}/\nu_5$, $\nu_4 + \nu_5/\nu_3$, $\nu_7 + \nu_9/\nu_4$, $\nu_8 + \nu_9/\nu_5$, $\nu_{10} + \nu_{12}/\nu_4$.

In the wavenumber region from 5950 to 6250 cm^{-1}, there is a resonant polyad involving 12 bands detailed by the C−H overtones $2\nu_i$ ($i = 1$, 2, and 3), their combination bands $\nu_i + \nu_j$ ($i = 1$, 2; $j = 2$, 3), and three quanta combination bands $\nu_i + \nu_j + \nu_k$ ($i = 1$, 2, 3; $j = 4$; $k = 5$, 6). This resonant polyad

TABLE 8: Theoretical Rotational Constants (in cm^{-1}) of $H_2C{=}CHF$: Comparison with Experimental Data

vibrational state	parameter	calculated [a]	observed	(O. − C.) %[b]
ground	*A*	2.153 977 9	2.154 313 1[c]	0.02
	B	0.353 004 3	0.354 808 20[c]	0.51
	C	0.302 807 9	0.304 144 91[c]	0.44
$v_1 = 1$	*A*	2.147 637 3	−	−
	B	0.352 544 2	−	−
	C	0.302 396 3	−	−
$v_2 = 1$	*A*	2.147 351 3	−	−
	B	0.352 659 0	−	−
	C	0.302 462 2	−	−
$v_3 = 1$	*A*	2.145 982 4	−	−
	B	0.352 720 6	−	−
	C	0.302 430 0	−	−
$v_4 = 1$	*A*	2.144 726 0	2.143 574[d]	−0.05
	B	0.351 846 8	0.353 469 5[d]	0.46
	C	0.301 610 2	0.302 945 2[d]	0.44
$v_5 = 1$	*A*	2.162 485 9	2.167 68[e]	0.24
	B	0.353 609 4	0.355 282[e]	0.47
	C	0.302 569 5	0.303 892[e]	0.44
$v_6 = 1$	*A*	2.146 672 6	2.147 330[e]	0.03
	B	0.353 997 0	0.355 780[e]	0.50
	C	0.302 965 7	0.304 274[e]	0.43
$v_7 = 1$	*A*	2.161 758 5	2.160 768 4[c]	−0.05
	B	0.352 431 8	0.354 289 92[c]	0.52
	C	0.301 364 4	0.302 708 04[c]	0.44
$v_8 = 1$	*A*	2.179 351 1	2.190 790[f]	0.52
	B	0.344 784 2	0.353 940 4[f]	2.59
	C	0.302 070 2	0.303 343 01[f]	0.42
$v_9 = 1$	*A*	2.152 028 3	2.151 208 69[g]	−0.04
	B	0.352 937 7	0.354 653 821[g]	0.48
	C	0.302 477 2	0.303 760 709[g]	0.42
$v_{10} = 1$	*A*	2.149 282 1	2.137 170 8[f]	−0.57
	B	0.360 169 4	0.354 465 77[f]	−1.61
	C	0.30 305 10	0.304 375 46[f]	0.03
$v_{11} = 1$	*A*	2.114 887 2	2.115 590[f]	0.03
	B	0.352 378 0	0.354 052 2[f]	0.47
	C	0.303 024 0	0.304 355 60[f]	0.44
$v_{12} = 1$	*A*	2.153 422 9	2.153 348 6[h]	0.00
	B	0.352 534 3	0.354 358 60[h]	0.51
	C	0.302 919 5	0.304 272 27[h]	0.44

[a] From the hybrid anharmonic force field (see text). [b] (O. − C.) % = (obs. − calc.) * 100/obs. [c] Reference 8. [d] Reference 14. [e] Reference 16. [f] Reference 17. [g] Reference 15. [h] Reference 13.

involves Darling−Dennison resonances defined from the following matrix elements[31]

$$\langle v_i+2, v_j|H|v_i, v_j+2\rangle = \frac{K_{iijj}}{4}[(v_i+1)(v_i+2)(v_j+1)(v_j+2)]^{(1/2)} \quad (6)$$

the second-order terms[32]

$$\langle v_i+1, v_j-1|H|v_i, v_j\rangle = \frac{K_{ijjj}}{4}[(v_i+1)(v_j-1)^2 v_j]^{(1/2)} \quad (7)$$

and the Fermi resonance matrix elements[30]

$$\langle v_i, v_j, v_k|H|v_i-1, v_j+1, v_k+1\rangle = \varphi_{ijk}[v_i(v_j+1)(v_k+1)/8]^{(1/2)} \quad (8)$$

After diagonalization of the resonant matrix, three main wavenumbers regions could be identified:
5950−6000 cm^{-1} containing the $2\nu_3$ and other three-quanta combination bands;
6000−6150 cm^{-1} with $\nu_1 + \nu_3$, $2\nu_2$, $\nu_2 + \nu_3$, and many other three-quanta bands;
6200−6250 cm^{-1} with $\nu_1 + \nu_2$ and $2\nu_1$.

From inspection of the eigenvectors, one finds that many transitions involving the combination bands are strongly mixed and in some instances the assignment becomes a matter of taste.

TABLE 9: Experimental and Calculated Quartic and Sextic Centrifugal Distortion Constants (cm^{-1}) for $H_2C{=}CHF$

	obs.[a]	calc.	(O. − C.) %[b]
$\Delta_J \times 10^6$	0.281 26	0.278 50	0.98
$\Delta_{JK} \times 10^5$	−0.253 7	−0.265 63	−4.70
$\Delta_K \times 10^4$	0.443 67	0.452 55	−2.00
$\delta_J \times 10^7$	0.589 1	0.580 00	1.54
$\delta_K \times 10^5$	0.118 6	0.110 28	7.02
$\Phi_J \times 10^{12}$	0.47	0.497 56	−5.86
$\Phi_{JK} \times 10^{12}$	−	−0.147 83	−
$\Phi_{KJ} \times 10^9$	−0.223	−0.240 40	−7.80
$\Phi_K \times 10^8$	0.259	0.278 61	−7.57
$\phi_J \times 10^{12}$	0.217	0.211 50	2.53
$\phi_{JK} \times 10^{11}$	−	0.268 19	−
$\phi_K \times 10^9$	0.46	0.444 60	3.35

[a] Reference 8. [b] (O. − C.) % = (obs. − calc.) * 100/obs.

The experimental and *ab initio* rotational constants are compared in Table 8. The calculated values have been computed with the hybrid anharmonic force field previously described. The agreement between calculated and experimental values is good, and all the constants exhibit comparable small discrepancies.

Table 9 contains the equilibrium quartic centrifugal distortion constants (A-reduction[33]) calculated from the quadratic force

field (CCSD(T)/cc-pVQZ) and compares them with their experimental counterparts. The equilibrium sextic centrifugal distortion constants (A-reduction) calculated from CCSD(T)/cc-pVTZ cubic force field are also reported in Table 9. Comparisons with the available experimental ground-state constants for quartic and sextic terms reveal a good agreement between theory and experiment.

5. Conclusion

A detailed study of the infrared spectral characteristics of vinyl fluoride has been carried out both experimentally and theoretically. The observed absorption features have been identified as fundamentals, overtones, and up to three quanta combination bands leading to an almost complete understanding of the vibrational spectra within the range 400−8000 cm^{-1}. The partially resolved rotational structures have also been analyzed, and preliminary rotational parameters for the ν_1 and ν_2 fundamentals and some combination bands have been determined. The integrated absorption cross sections have been measured for the first time; the obtained values well agree with those retrieved by the *ab initio* calculations carried out here.

The quantum mechanic calculations have led to the determination of an hybrid force field from which accurate values of anharmonicity constants and rotational and centrifugal distortion parameters have been obtained. The comparison of the theoretical rotational constants with the experimentally available ones shows a very remarkable agreement, suggesting that the hybrid force field here determined represents a very realistic description.

The obtained results provide basic information which can be used for high-resolution infrared studies as well as to improve theoretical investigations about the reactivity of vinyl fluoride toward hydroxyl radical and ozone. In addition, the absorption band intensities could also be useful for global climate calculation by radiative transfer models.

Acknowledgment. The authors acknowledge gratefully the financial support by PRIN 2007 (project: *Trasferimenti di energia, carica e molecole in sistemi complessi*) and the High Performance Systems Division of the CINECA Supercomputer Centre (Interuniversity Consortium) for support in the utilization of computer resources.

References and Notes

(1) Torkington, P.; Thompson, H. W. *Trans. Faraday Soc.* **1945**, *41*, 236–245.
(2) Scherer, J. R.; Potts, W. J. *J. Chem. Phys.* **1959**, *31*, 1691–1692.
(3) McKean, D. C. *Spectrochim. Acta* **1975**, *31A*, 1167–1186.
(4) Elst, R.; Oskam, A. *J. Mol. Spectrosc.* **1971**, *39*, 357–363.
(5) Morgan, H. W.; Goldstein, J. H. *J. Chem. Phys.* **1959**, *30*, 1025–1028.
(6) Gerry, M. C. L. *J. Mol. Spectrosc.* **1973**, *45*, 71–78.
(7) Hayashi, M.; Inagusa, T. *J. Mol. Spectrosc.* **1989**, *138*, 135–140.
(8) Stoppa, P.; Giorgianni, S.; Gambi, A.; De Lorenzi, A.; Ghersetti, S. *Mol. Phys.* **1995**, *84*, 281–290.
(9) Smith, B. J., Jr.; Radom, L. *J. Chem. Phys.* **1992**, *97*, 6113–6120.
(10) Demaison, J. *J. Mol. Spectrosc.* **2006**, *239*, 201–207.
(11) Sekušak, S.; Liedl, K. R.; Sabljić, A. *J. Phys. Chem. A* **1998**, *102*, 1583–1594.
(12) Ljubić, I.; Sabljić, A. *J. Phys. Chem. A* **2002**, *106*, 4745–4757.
(13) Gambi, A.; De Lorenzi, A.; Giorgianni, S.; Stoppa, P. *J. Mol. Spectrosc.* **1995**, *171*, 504–512.
(14) De Lorenzi, A.; Giorgianni, S.; Stoppa, P.; Gambi, A. *Mol. Phys.* **1996**, *87*, 581–591.
(15) Gambi, A.; De Lorenzi, A.; Giorgianni, S. *J. Mol. Spectrosc.* **1997**, *182*, 378–384.
(16) Stoppa, P.; Pietropolli Charmet, A.; Visinoni, R.; Giorgianni, S. *Mol. Phys.* **2005**, *103*, 657–666.
(17) Tasinato, N.; Stoppa, P.; Pietropolli Charmet, A.; Giorgianni, S.; Gambi, A. *J. Phys. Chem. A* **2006**, *110*, 13412–13418.
(18) Purvis, G. D., III; Bartlett, R. J. *J. Chem. Phys.* **1982**, *76*, 1910–1918.
(19) Raghavachari, K.; Trucks, G. W.; Pople, J. A.; Head-Gordon, M. *Chem. Phys. Lett.* **1989**, *157*, 479–483.
(20) Dunning, T. H., Jr *J. Chem. Phys.* **1989**, *90*, 1007–1023.
(21) Wilson, A. K.; Woon, D. E.; Peterson, K. A.; Dunning, T. H., Jr *J. Chem. Phys.* **1999**, *110*, 7667–7676.
(22) Schneider, W.; Thiel, W. *Chem. Phys. Lett.* **1989**, *157*, 367–373.
(23) Stanton, J. F.; Gauss, J.; Watts, J. D.; Szalay, P. G.; Bartlett, R. J. with contributions from Auer, A. A.; Bernholdt, D. E.; Christiansen, O.; Harding, M. E.; Heckert, M.; Heun, O.; Huber, C.; Jonsson, D.; Jusélius, J.; Lauderdale, W. J.; Metzroth, T.; Michauk, C.; O'Neill, D. P.; Price, D. R.; Ruud, K.; Schiffmann, F.; Varner, M. E.; Vázquez, J. and the integral packages MOLECULE (Almlöf, J. and Taylor, P. R.), PROPS (Taylor, P. R.), and ABACUS (Helgaker, T.; Jensen, H. J. Aa.; Jørgensen, P. and Olsen, J.). For the current version, see http://www.aces2.de.
(24) MOLPRO (version 2002.6) is a package of ab initio programs written by Werner, H. -J.; Knowles, P. J. with contributions of Amos, R. D.; Bernhardsson, A.; Celani, P.; Cooper, D. L.; Deegan, M. J. O.; Dobbyn, A. J.; Eckert, F.; Hampel, C.; Hetzer, G.; Korona, T.; Lindh, R.; Lloyd, A. W.; McNicholas, S. J.; Manby, F. R.; Meyer, W.; Mura, M. E.; Nicklass, A.; Palmieri, P.; Pitzer, R.; Rauhut, G.; Schütz, M.; Stoll, H.; Stone, A. J.; Tarroni, R.; Thorsteinsson, T.
(25) Eckert, F.; Pulay, P.; Werner, H.-J. *J. Comput. Chem.* **1997**, *18*, 1473–1483.
(26) Nemtchinov, V.; Varanasi, P. *J. Quant. Spectrosc. Radiat. Transfer* **2004**, *83*, 285–294.
(27) Bak, K. L.; Gauss, J.; Jørgensen, P.; Olsen, J.; Helgaker, T.; Stanton, J. F. *J. Chem. Phys.* **2001**, *114*, 6548–6556.
(28) Allen, W. D.; Császár, A. G.; Horner, D. A. *J. Am. Chem. Soc.* **1992**, *114*, 6834–6849.
(29) Mills, I. M. *Molecular Spectroscopy: Modern Research*; Narahari Rao, K.; Mathews, C. W., Eds.; Acadamic: New York, 1972.
(30) Papoušek,D.; Aliev,M. R. *Molecular Vibrational-Rotational Spectra*; Elsevier: Amsterdam, 1982.
(31) Mills, I. M.; Robiette, A. G. *Mol. Phys.* **1985**, *56*, 743–765.
(32) Lehmann, K. K. *Mol. Phys.* **1989**, *66*, 1129–1137. Erratum 1992, *75*, 739.
(33) Watson, J. K. G. *Vibrational Spectra and Structure*; Elsevier: Amsterdam, 1977; Vol. 6.

JP808556E